Non-monotonic behaviour in relaxation dynamics of image restoration

2003 J. Phys. A: Math. Gen. 36 11011

(http://iopscience.iop.org/0305-4470/36/43/024)

INSTITUTE OF PHYSICS PUBLISHING JOURNAL OF PHYSICS A: MATHEMATICAL AND GENERAL

J. Phys. A: Math. Gen. **36** (2003) 11011–11021 PII: S0305-4470(03)61615-X

Non-monotonic behaviour in relaxation dynamics of image restoration

Tomoko Ozeki[1] **and Masato Okada**[1,2]

[1] RIKEN Brain Science Institute, Wako, Saitama 351-0198, Japan
[2] Intelligent Cooperation and Control, PRESTO, JST, Saitama 351-0198, Japan

E-mail: tomoko@brain.riken.go.jp and okada@brain.riken.go.jp

Received 31 March 2003
Published 15 October 2003
Online at stacks.iop.org/JPhysA/36/11011

Abstract

We have investigated the relaxation dynamics of image restoration through a Bayesian approach. The relaxation dynamics is much faster at zero temperature than at the Nishimori temperature where the pixel-wise error rate is minimized in equilibrium. At low temperature, we observed non-monotonic development of the overlap. We suggest that the optimal performance is realized through premature termination in the relaxation processes in the case of the infinite-range model. We also performed Markov chain Monte Carlo simulations to clarify the underlying mechanism of non-trivial behaviour at low temperature by checking the local field distributions of each pixel.

PACS numbers: 02.50.−r, 05.20.−y, 05.50.+q, 75.10.Nr, 89.70.+c

1. Introduction

Equilibrium statistical mechanics has been applied to probabilistic information processing such as image restoration [1–9], error-correcting codes [5, 10–12] and code-division multiple access (CDMA) multi-user demodulation [13, 14] based on Bayesian statistics [15]. This approach enables us to analytically estimate the performance of the results obtained for these problems and the dependence of the error rate on the restoration/decoding temperature [5]. However, only static properties of the solutions can be investigated through this approach.

Markov chain Monte Carlo (MCMC) has been used to obtain solutions which maximize the posterior probability (MAP) or the posterior marginals (MPM) within the framework of Bayesian inference. The MPM estimate is also called the finite-temperature restoration whereas the MAP estimate corresponds to the zero-temperature restoration. When the image restoration is performed at a specific temperature, called the Nishimori temperature [5, 15, 16], the pixel-wise error rate can be minimized. However, it is unclear whether the Nishimori temperature is optimal in the MCMC relaxation processes. It is important to describe the dynamics in order to examine dynamical properties such as the dependence of the relaxation

speed on the temperature and the transient behaviour of the system. However, much less work has been done regarding the analysis of MCMC relaxation processes to get the MPM estimate [6, 17, 18].

In this paper, the relaxation processes of image restoration are investigated by means of statistical mechanics. Starting from the microscopic time evolution equations of the system, we have analysed the dynamics using a few macroscopic variables which describe the system. In section 2, we describe the model of image restoration within a Bayesian inference framework. In section 3, we explain the mean-field theory of image restoration for equilibrium properties and non-equilibrium dynamics. In section 4, we analyse the dynamics of restoration by describing the time evolution equations of macrovariables. We have performed MCMC simulations to gain an intuitive understanding of the underlying mechanism of the non-trivial behaviour at low temperature.

We have also examined two-dimensional images which are difficult to investigate analytically.

2. Model

Let us consider the problem in which we estimate the original image $\boldsymbol{\xi} = (\xi_1, \ldots, \xi_N)$, $\xi_i = \pm 1$ from the corrupted image $\boldsymbol{\tau} = (\tau_1, \ldots, \tau_N)$. Under the framework of Bayesian inference, we first have to assume a corruption process. One corruption model is the binary symmetric channel (BSC) where τ_i is equal to $\pm\xi_i$ with probabilities $1 - p_r$ and p_r respectively. The probability can be written as

$$P(\boldsymbol{\tau}|\boldsymbol{\xi}) = \frac{\exp\left(\beta_\tau \sum_i \tau_i \xi_i\right)}{(2\cosh\beta_\tau)^N} \tag{1}$$

where $\beta_\tau = \frac{1}{2}\ln\frac{1-p_r}{p_r}$.

Another corruption model is the Gaussian channel,

$$P(\boldsymbol{\tau}|\boldsymbol{\xi}) = \frac{1}{(\sqrt{2\pi}\tau)^N}\exp\left[-\sum_i \frac{(\tau_i - \tau_0\xi_i)^2}{2\tau^2}\right]. \tag{2}$$

Hereafter, the Gaussian channel model is assumed. We also assume that the original images are generated according to the prior probability:

$$P_s(\boldsymbol{\xi}) = \frac{\exp\left(\beta_s \sum_{\langle ij\rangle} \xi_i \xi_j\right)}{Z(\beta_s)} \tag{3}$$

where $\sum_{\langle ij\rangle}$ denotes the summation over the couplings between all pixels for the infinite-range model and the couplings between nearest neighbours for two-dimensional images, respectively. $\beta_s (= 1/T_s)$ is the inverse temperature at which the original image is generated.

According to the Bayes formula, the posterior probability of the original image $\boldsymbol{\xi}$ can be obtained as

$$\begin{aligned} P(\boldsymbol{\xi}|\boldsymbol{\tau}) &= \frac{P(\boldsymbol{\tau}|\boldsymbol{\xi})P_s(\boldsymbol{\xi})}{\mathrm{Tr}_\xi P(\boldsymbol{\tau}|\boldsymbol{\xi})P_s(\boldsymbol{\xi})} \\ &= \frac{\exp\left(\beta_s \sum_{\langle ij\rangle}\xi_i\xi_j + \frac{\tau_0}{\tau^2}\sum_i \tau_i\xi_i\right)}{\mathrm{Tr}_\xi \exp\left(\beta_s \sum_{\langle ij\rangle}\xi_i\xi_j + \frac{\tau_0}{\tau^2}\sum_i \tau_i\xi_i\right)}. \end{aligned}$$

When image restoration is performed, parameters such as β_s, τ_0 and τ are not provided beforehand, so we have to estimate or adjust these parameters. Therefore, we use the notation

of $\beta_m (= 1/T_m)$ and h instead of β_s and τ_0/τ^2, respectively. We denote the restored image as $\boldsymbol{\sigma}$ to avoid any confusion with the original image, thus the posterior probability is given by

$$P(\boldsymbol{\sigma}|\boldsymbol{\tau}) = \frac{\exp\left(\beta_m \sum_{\langle ij\rangle} \sigma_i\sigma_j + h\sum_i \tau_i\sigma_i\right)}{\mathrm{Tr}_{\boldsymbol{\sigma}} \exp\left(\beta_m \sum_{\langle ij\rangle} \sigma_i\sigma_j + h\sum_i \tau_i\sigma_i\right)}. \tag{4}$$

We can recognize the formal similarity to the Boltzmann factor of an Ising spin system with ferromagnetic interactions and random external fields.

The MAP estimate is a method for estimating an original image from the posterior probability. The maximization process of the posterior probability is equivalent to a ground-state search of an Ising spin system with the Hamiltonian

$$H(\boldsymbol{\sigma}) = -\beta_m \sum_{\langle ij\rangle} \sigma_i\sigma_j - h\sum_i \tau_i\sigma_i. \tag{5}$$

On the other hand, the MPM estimate is given by maximization of the posterior marginals,

$$P(\sigma_i|\boldsymbol{\tau}) = \frac{\mathrm{Tr}_{\boldsymbol{\sigma}(\neq\sigma_i)} \exp\left(\beta_m \sum \sigma_i\sigma_j + h\sum_i \tau_i\sigma_i\right)}{\mathrm{Tr}_{\boldsymbol{\sigma}} \exp\left(\beta_m \sum \sigma_i\sigma_j + h\sum_i \tau_i\sigma_i\right)}. \tag{6}$$

In this case, the estimate of each pixel is given by

$$\hat{\xi}_i = \mathrm{sgn}\left[\sum_{\sigma_i=\pm 1} \sigma_i P(\sigma_i|\boldsymbol{\tau})\right] = \mathrm{sgn}\langle\sigma_i\rangle \tag{7}$$

which minimizes the pixel-wise error rate.

3. Mean-field theory

3.1. Equilibrium

One of our goals is to obtain the average overlap between an original image and the corresponding restored image,

$$\begin{aligned} M(\beta_m, h) &\equiv \langle \xi_i \mathrm{sgn}\langle\sigma_i\rangle | \beta_m^*, h^*\rangle \\ &\equiv \int \mathrm{d}\boldsymbol{\tau} \sum_{\boldsymbol{\xi}} P_s(\boldsymbol{\xi}) P(\boldsymbol{\tau}|\boldsymbol{\xi}) \xi_i \mathrm{sgn}\langle\sigma_i\rangle \end{aligned} \tag{8}$$

so that we can use it as a performance measure, where β_m^* and h^* are the true parameters equal to β_s and τ_0/τ^2, respectively. Nishimori and Wong [5] have derived a rigorous inequality,

$$M(\beta_m, h) \leqslant M(\beta_m^*, h^*) = M(\beta_s, \tau_0/\tau^2). \tag{9}$$

We refer to the parameters $(\beta_m, h) = (\beta_m^*, h^*)$ as the Nishimori temperature, which corresponds to the Nishimori line in spin-glass theory [16].

The equilibrium properties of such a system have been investigated through the replica method for the infinite-range model [5],

$$H = -\frac{\beta_m}{N} \sum_{i<j} \sigma_i\sigma_j - h\sum_i \tau_i\sigma_i \tag{10}$$

where the summation is carried out for all pixel pairs. Static properties are described using the order parameters

$$m_0 \equiv \frac{1}{N}\sum_i \xi_i = \tanh(\beta_s m_0)$$

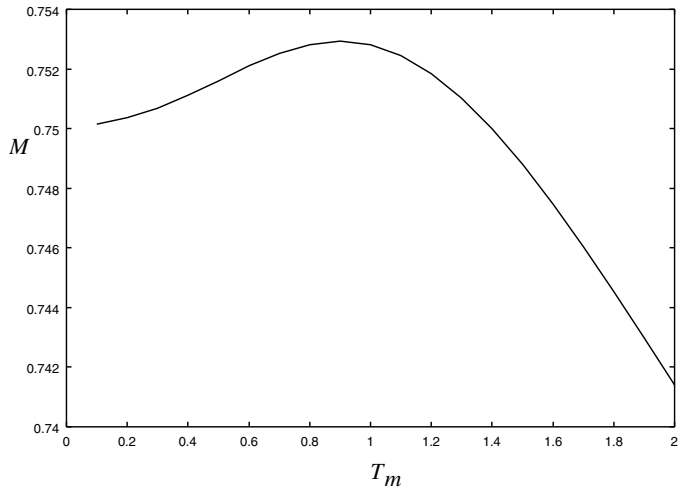

Figure 1. Temperature dependence of the average overlap M: $T_s = 0.9$, $\tau_0 = \tau = 1.0$, and h/β_m was held constant relative to the optimal value, $(\tau_0/\tau^2)/\beta_s$.

and

$$m \equiv \frac{1}{N}\sum_i \sigma_i = \frac{\mathrm{Tr}_\xi \int Dx\, \mathrm{e}^{\beta_s m_0 \xi} \tanh(\beta_m m + \tau h x + \tau_0 h \xi)}{2\cosh(\beta_s m_0)}$$

where $Dx = 1/\sqrt{2\pi}\, \mathrm{e}^{-\frac{1}{2}x^2}\, \mathrm{d}x$. The overlap M is given by

$$M \equiv \frac{1}{N}\sum_i \xi_i \hat{\xi}_i = \frac{\mathrm{Tr}_\xi \int Dx\, \mathrm{e}^{\beta_s m_0 \xi}\, \xi\, \mathrm{sgn}(\beta_m m + \tau h x + \tau_0 h \xi)}{2\cosh(\beta_s m_0)}. \tag{11}$$

Hereafter, we consider the behaviour of the overlap as a function of β_m when h/β_m is held constant relative to the optimal value $(\tau_0/\tau^2)/\beta_s$. The overlap shows non-monotonic behaviour which reaches its extreme at $T_m = T_s$ in figure 1; this temperature corresponds to the Nishimori temperature [5]. However, it is non-trivial whether the Nishimori temperature is optimal in the relaxation processes in the sense that the relaxation is fastest. Therefore, we analysed the relaxation processes as discussed below.

3.2. Dynamics

We derived differential equations for the infinite-range model with respect to macroscopic order parameters as was done by Inoue and Tanaka [17]. The transition probability of the kth spin, which has the Hamiltonian (5), is given by

$$w_k(\boldsymbol{\sigma}) = \tfrac{1}{2}\{1 - \sigma_k \tanh[h_k(\boldsymbol{\sigma})]\} \tag{12}$$

where $h_k(\boldsymbol{\sigma})$ is the local field of the kth spin and $h_k(\boldsymbol{\sigma}) = \frac{\beta_m}{N}\sum_{j\neq k}\sigma_j + h\tau_k$. We rescaled the coupling as $1/N$ to obtain a proper thermodynamic limit. Starting from the master equation

$$\frac{\mathrm{d}p_t(\boldsymbol{\sigma})}{\mathrm{d}t} = \sum_{k=1}^{N}[p_t(F_k(\boldsymbol{\sigma}))w_k(F_k(\boldsymbol{\sigma})) - p_t(\boldsymbol{\sigma})w_k(\boldsymbol{\sigma})] \tag{13}$$

the system dynamics can be described using the time development equations for macrovariables m and $a \equiv \frac{1}{N}\sum \tau_i \sigma_i$. Here, F_k is a spin-flip operator, and $F_k\Phi(\boldsymbol{\sigma}) \equiv$

$\Phi(\sigma_1, \ldots, -\sigma_k, \ldots, \sigma_N)$. The probability that the system has order parameters m and a is given by

$$P_t(m, a) = \sum_{\sigma} P_t(\boldsymbol{\sigma})\delta(m - m(\boldsymbol{\sigma}))\delta(a - a(\boldsymbol{\sigma})). \tag{14}$$

The time evolution equation of the macroscopic probability distribution is obtained by differentiating $P_t(m, a)$ with t, substituting through equation (13) and Taylor expansion:

$$\begin{aligned}\frac{\mathrm{d}P_t(m,a)}{\mathrm{d}t} = {} & \frac{\partial}{\partial m}P_t(m,a)\left\{m - \frac{\sum_\xi \mathrm{e}^{\beta_s m_0 \xi}}{2\cosh(\beta_s m_0)}\int_{-\infty}^{\infty} Dx \tanh(Jm + h\tau x + h\tau_0\xi)\right\} \\ & + \frac{\partial}{\partial a}P_t(m,a)\left\{a - \frac{\sum_\xi \mathrm{e}^{\beta_s m_0 \xi}}{2\cosh(\beta_s m_0)}\int_{-\infty}^{\infty} Dx(\tau x + \tau_0\xi)\tanh(Jm + h\tau x + h\tau_0\xi)\right\} \\ & + O(N^{-1}).\end{aligned} \tag{15}$$

At the limit $N \to \infty$, equation (15) acquires the Liouville form and describes the deterministic flow at the macroscopic level (m, a). The time-dependent behaviour of the macrovariables is given by

$$\frac{\mathrm{d}m}{\mathrm{d}t} = -m + \frac{\mathrm{Tr}_\xi \int Dx\, \mathrm{e}^{\beta_s m_0 \xi}\tanh(\beta_m m + \tau h x + \tau_0 h\xi)}{2\cosh(\beta_s m_0)} \tag{16}$$

and

$$\frac{\mathrm{d}a}{\mathrm{d}t} = -a + \frac{\mathrm{Tr}_\xi \int Dx\, \mathrm{e}^{\beta_s m_0 \xi}(\tau x + \tau_0\xi)\tanh(\beta_m m + \tau h x + \tau_0 h\xi)}{2\cosh(\beta_s m_0)}. \tag{17}$$

Here the equation for m is independent of a, so the time-dependent behaviour of the system is given only by equation (16). The overlap M is obtained by solving the equation for m and substituting m into equation (11).

4. Results

4.1. Theory

The dependence of the time evolution of the overlap M on the restoration temperature is shown in figure 2. The temperature $T_m = 1/\beta_m$ was set to 0.1 (low temperature), 0.9 ($=1/\beta_s$, the Nishimori temperature) and 2.0 (high temperature). The relaxation occurred more rapidly at low temperature than at the Nishimori temperature where the pixel-wise error rate is optimal in equilibrium. The optimal overlap of the Nishimori temperature is achieved at an early stage of the relaxation process at low temperature. As for the dynamics of m, the relaxation occurs more quickly at low temperature and passes through the equilibrium value m_{opt} of the Nishimori temperature in figure 3. The overlap M is a non-monotonic function of m in figure 4 and reaches a maximum at $m = m_{\mathrm{opt}}$. This causes the non-monotonic behaviour of M. At low temperature, m reaches the optimal m_{opt} more quickly (figure 3), and M reaches its maximum value early in the time evolution.

We can intuitively understand this mechanism by considering the time development of the local field distributions. Figure 5 shows the time evolution of local field distributions obtained from MCMC simulations with $N = 100\,000$, $T_s = 0.9$ and $\tau_0 = \tau = 1.0$. True distributions (inset) were fitted using Gaussian distributions to see how the distribution changed over time. For the infinite-range model, the local field of each spin is represented in terms of magnetization m: $h_i \simeq \beta_m m + h\tau_i$. The second term is fixed during the time development and gives two Gaussian distributions, one for $\xi_i = 1$ and another for $\xi_i = -1$, since $\tau_i = \tau_0\xi_i + \tau z$, where z

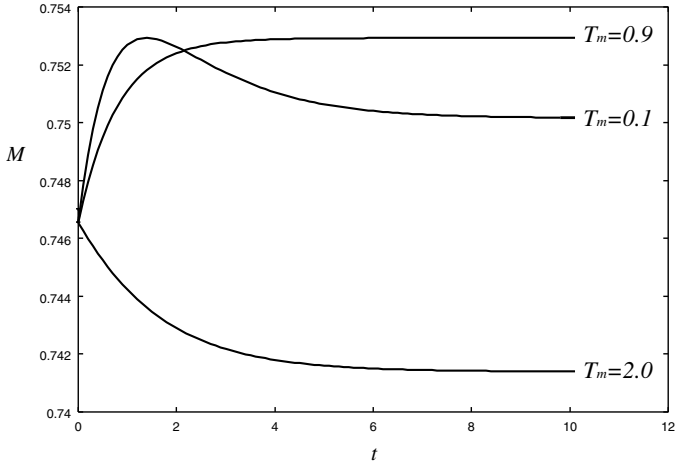

Figure 2. Time evolution of the overlap M: $T_m = 0.1$, $T_m = 0.9\,(= T_s$, the Nishimori temperature), $T_m = 2.0$, $\tau_0 = \tau = 1.0$, h/β_m was held constant at the optimal value, $(\tau_0/\tau^2)/\beta_s$.

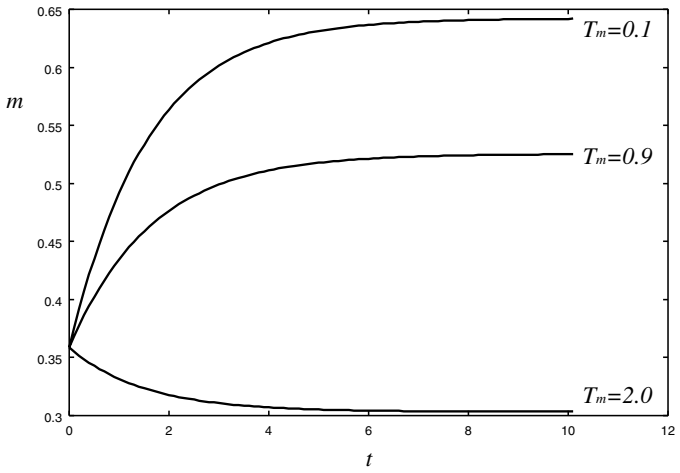

Figure 3. Time evolution of the order parameter m: $T_m = 0.1$, $T_m = 0.9\,(= T_s$, the Nishimori temperature), $T_m = 2.0$.

is Gaussian with mean 0 and variance 1. Over time, m in the first term approaches 1 and the peaks of both distributions shift to the right (figure 5). At low temperature, starting from the initial distributions (dotted lines) at $t = 0$, the distributions for both $\xi_i = 1$ and $\xi_i = -1$ shift to the right. Because of this shift, the error rate increases in the distribution for $\xi_i = -1$ since the estimated pixel value is given by $\hat{\xi}_i = \mathrm{sgn}(h_i)$. However, the error rate in the distribution for $\xi_i = 1$ decreases. The magnetization m, or the state which gives the minimal error rate, is the equilibrium value m_{opt} at the Nishimori temperature. Over time, the distribution passes through equilibrium at the Nishimori temperature (solid lines). When the restoration is done at low temperature, m passes through m_{opt} in the dynamics and becomes larger than this value. As a result, M shows non-monotonic behaviour.

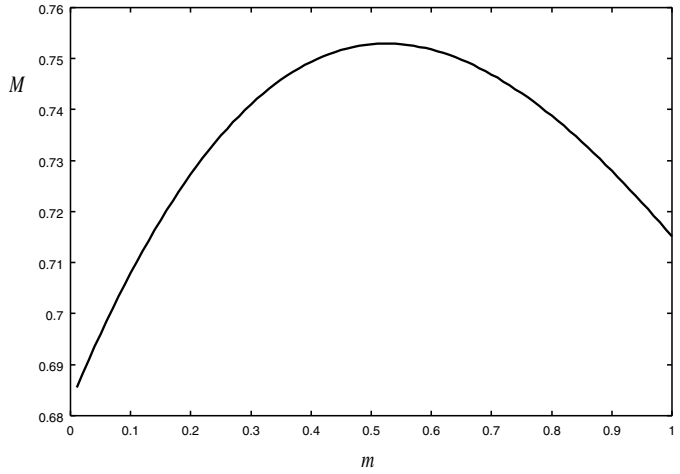

Figure 4. Dependence of the overlap M on m.

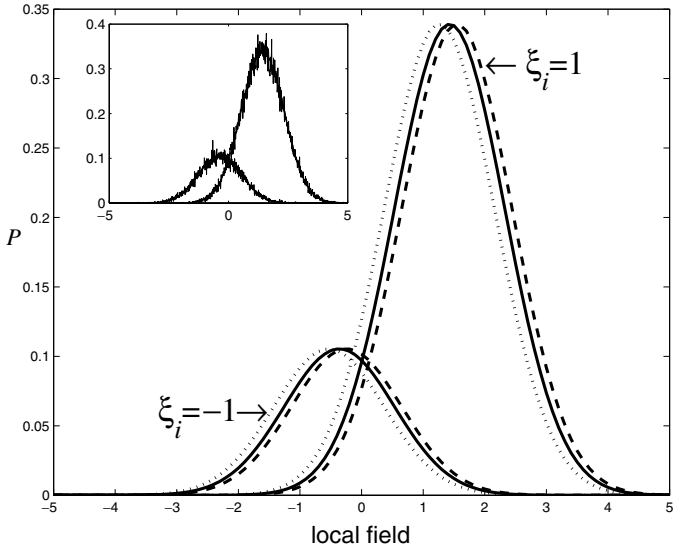

Figure 5. Time evolution of the local field distribution for the infinite-range model: these are the results of MCMC simulations with $N = 100\,000$, $T_s = 0.9$ and $\tau_0 = \tau = 1.0$. h/β_m was kept constant at the optimal value $(\tau_0/\tau^2)/\beta_s$. True distributions (inset) were fitted according to Gaussian distributions. Solid lines show the equilibrium local field distributions at the Nishimori temperature ($T_m = 0.9$). At low temperature ($T_m = 0.1$), starting from the initial distributions (dotted lines) at $t = 0$, the distributions for both $\xi_i = 1$ and $\xi_i = -1$ shifted to the right (dashed lines at $t = 10$). In the middle of the time evolution, the distribution passed through the equilibrium distribution at the Nishimori temperature. Because of this shift, the probability of error decreased in the distribution for $\xi_i = 1$, whereas for $\xi_i = -1$ the error increased.

These results suggest that at low temperature, the system transiently passes through the optimal state before reaching equilibrium. This means that the optimal solution can be obtained through premature termination of the system, at least in the case of the infinite-range model. We can obtain the timing of termination theoretically if we know the properties of

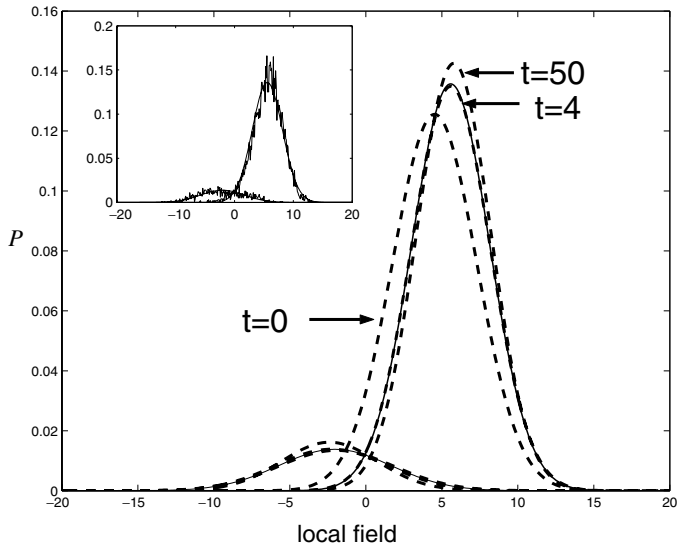

Figure 6. Time evolution of the local field distribution for the two-dimensional model. These are MCMC simulation results with $N = 100 \times 100$, $T_s = 2.2$ and $\tau_0 = \tau = 1.0$; h/β_m was kept constant relative to the optimal value, $(\tau_0/\tau^2)/\beta_s$. True distributions (inset) were fitted according to Gaussian distributions. Solid lines show the equilibrium local field distributions at the Nishimori temperature ($T_s = 2.2$). Dashed lines represent the time evolution of distributions at low temperature ($T_m = 1.0$). Time is shown as a parameter. At low temperature, starting from the initial distributions at $t = 0$, both of the distributions approach that of the Nishimori temperature and are very similar at $t = 4$.

noisy channels, such as the spin-flip probabilities. We can thus design a criterion to use for terminating the dynamics before they reach equilibrium. Specifically, by solving equation (16), we can predict the dynamical properties shown in figure 2 if we know the hyperparameters.

4.2. Two-dimensional system

It is interesting to see whether the non-monotonic behaviour at low temperature would hold in the case of a two-dimensional image. However, a two-dimensional system corresponds to a two-dimensional random field Ising model, which is difficult to investigate analytically. We therefore performed Monte Carlo simulations to investigate the restoration of two-dimensional images.

We generated the original image ($N = 100 \times 100$) by relaxing the Ising spin systems with nearest-neighbour interactions at the temperature $T_s = 2.15$ or 2.2 (below the critical temperature). We used the Gaussian channel model with $\tau_0 = 1$ and $\tau = 1$ for distortion. Starting from the distorted image, we performed image restoration by updating each pixel according to equation (12). Here, $h_k(\boldsymbol{\sigma}) = \beta_m \sum_{\text{n.n.}} \sigma_j + h\tau_k$.

Figure 6 shows the time evolution of the local field distribution during restoration at low temperature. At the beginning of the relaxation, the distribution approaches the equilibrium distribution at the Nishimori temperature and is overlapped at about $t = 4$. This figure suggests that the same mechanism as that of the infinite-range model is applicable to a two-dimensional system. In other words, the state of the system transiently passes through the Nishimori temperature optimal configuration at low temperature.

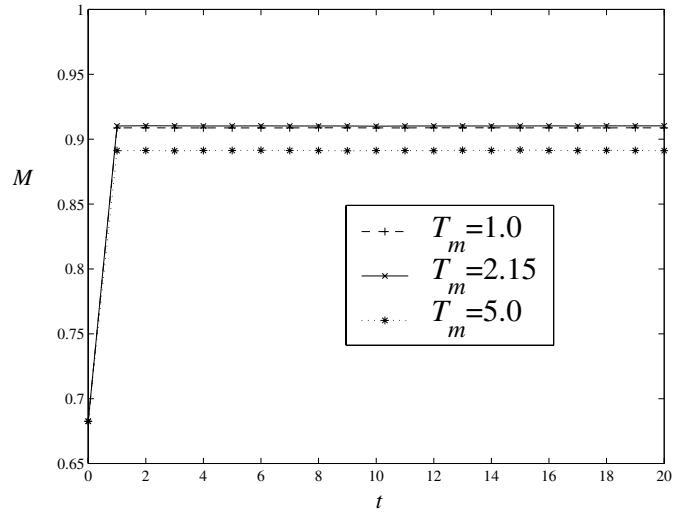

Figure 7. Time evolution of the overlap M: $T_s = 2.15$, $N = 100 \times 100$. For each sample, we performed 999 runs using different random numbers, stored the spin configurations at each time for each run and obtained the spin averages. We then averaged the time evolution of the overlap M over 100 samples.

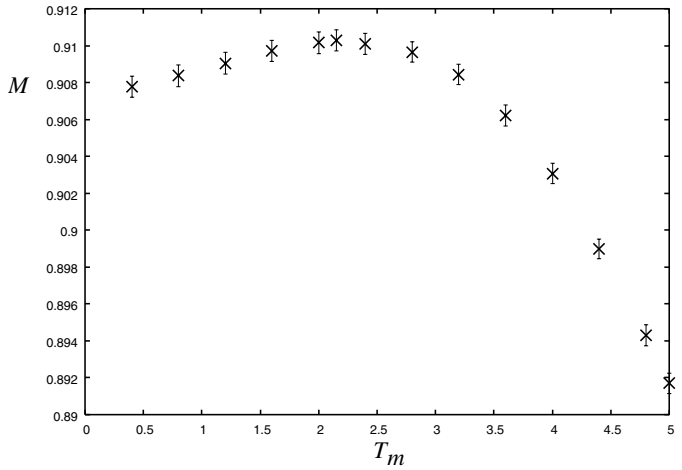

Figure 8. Temperature dependence of the overlap M: $T_s = 2.15$, $N = 100 \times 100$, 100 samples.

In the case of the infinite-range model, it is possible to measure the overlap by the local field. However, this is not true in the case of a two-dimensional system. The time evolution of overlap $M(\langle\sigma\rangle)$ is difficult to measure because the overlap is a function of the thermal average of the spins. If non-monotonic behaviour at low temperature in the infinite-range model is true for the two-dimensional system, it should occur at a very early stage ($t = 4$) in figure 6. Therefore, it is meaningless to measure the thermal average of spins by taking averages using a finite time window.

We prepared 100 samples for ξ and τ. For each sample, we performed $P(=999)$ runs using different random numbers, stored the spin configurations at each time for each run and

obtained the average $\langle \sigma_i^t \rangle \equiv \frac{1}{P} \sum_{m=1}^{P} \sigma_i^t(m)$. We then averaged the time evolution of the overlap M over 100 samples. (Figure 7 shows the time evolution of the overlap M.) We were unable to observe non-monotonic behaviour of the overlap at low temperature in the case of the two-dimensional system. One reason for this might be that the overlap M was almost constant at temperatures lower than the Nishimori temperature, as in figure 8. It was difficult to obtain statistically significant non-monotonic behaviour. We can still conclude, though, that there is at least a possibility that the system passes through the optimal state at the beginning of the relaxation at low temperature, as suggested by the time evolution of the local field distributions in figure 6.

5. Conclusion

In this paper, we have described the relaxation processes of image restoration by means of statistical mechanics.

An image can be restored much faster at low temperature than at the Nishimori temperature, and in the middle of the relaxation process the overlap M reaches a maximum value. This value is the same as the equilibrium solution for restoration at the Nishimori temperature. This suggests that the system goes through the optimal state in the MPM sense before reaching equilibrium, and that the premature termination of the system in the process is an effective means to obtain the optimal solution more quickly at least in the case of the infinite-range model. We can design a criterion according to which the dynamics are terminated before reaching equilibrium. Specifically, by solving equation (16), we can predict the dynamical properties as shown in figure 2 if we know the hyperparameters.

Acknowledgments

We thank Professor Hidetoshi Nishimori for reading the first version of this manuscript and giving us many useful comments. We are also grateful to Dr Yukiyasu Ozeki and Professor Yôhei Saika for our fruitful discussions with them. This study was partially supported by Grants-in-Aid for Scientific Research on Priority Areas No 14084212 and Grant-in-Aid for Scientific Research (C) No 14580438.

References

[1] Geman S and Geman D 1984 *IEEE Trans. Pattern Anal. Mach. Intell.* **6** 721
[2] Marroquin J, Mitter S and Poggio T 1987 *J. Am. Stat. Assoc.* **82** 76
[3] Pryce J M and Bruce A D 1995 *J. Phys. A: Math. Gen.* **28** 511
[4] Tanaka K and Morita T 1995 *Phys. Lett.* A **203** 122
[5] Nishimori H and Wong K Y M 1999 *Phys. Rev.* E **60** 132
[6] Saika Y and Nishimori H 2002 *J. Phys. Soc. Japan* **71** 1052
[7] Shouno H, Wada K and Okada M 2002 *J. Phys. Soc. Japan* **71** 2406
[8] Tsuzurugi J and Okada M 2002 *Phys. Rev.* E **66** 066704
[9] Tanaka K 2002 *J. Phys. A: Math. Gen.* **35** R81
[10] Sourlas N 1989 *Nature* **339** 693
[11] Ruján P 1993 *Phys. Rev. Lett.* **70** 2968
[12] Kabashima Y and Saad D 1999 *Europhys. Lett.* **45** 97
[13] Tanaka T 2001 *Europhys. Lett.* **54** 540

[14] Nishimori H 2002 *Europhys. Lett.* **57** 302
[15] Nishimori H 2001 *Statistical Physics of Spin Glasses and Information Processing: An Introduction* (Oxford: Oxford University Press)
[16] Nishimori H 1981 *Prog. Theor. Phys.* **66** 1169
[17] Inoue J and Tanaka K 2001 *Phys. Rev.* E **65** 0161251
[18] Inoue J and Carlucci D M 2001 *Phys. Rev.* E **64** 036121